



**HAL**  
open science

## Photocatalytic Degradation of Quinoline Yellow over Ag<sub>3</sub>PO<sub>4</sub>

Asma Tab, Mohamed Dahmane, Belabed Chemseddin, Bachir Bellal,  
Mohamed Trari, Claire Richard

► **To cite this version:**

Asma Tab, Mohamed Dahmane, Belabed Chemseddin, Bachir Bellal, Mohamed Trari, et al.. Photocatalytic Degradation of Quinoline Yellow over Ag<sub>3</sub>PO<sub>4</sub>. *Catalysts*, 2020, 10 (12), pp.1461-10.3390/catal10121461 . hal-03083579

**HAL Id: hal-03083579**

**<https://hal.science/hal-03083579>**

Submitted on 19 Dec 2020

**HAL** is a multi-disciplinary open access archive for the deposit and dissemination of scientific research documents, whether they are published or not. The documents may come from teaching and research institutions in France or abroad, or from public or private research centers.

L'archive ouverte pluridisciplinaire **HAL**, est destinée au dépôt et à la diffusion de documents scientifiques de niveau recherche, publiés ou non, émanant des établissements d'enseignement et de recherche français ou étrangers, des laboratoires publics ou privés.

# 1                    **Photocatalytic degradation of Quinoline Yellow over Ag<sub>3</sub>PO<sub>4</sub>**

2  
3                    Asma Tab<sup>a,b\*</sup>, Mohamad Dahmane<sup>a</sup>, Belabed Chemseddin<sup>c</sup>, Bachir Bellal<sup>d</sup>, Mohamed  
4                    Trari<sup>d</sup>, Claire Richard<sup>b\*</sup>

5  
6                    (a) Laboratory of Chromatography, Faculty of Chemistry, University of Science and  
7                    Technology Houari Boumediène, BP 32 El-Alia, 16111, Algiers, Algeria.

8  
9                    (b) Université Clermont Auvergne, CNRS, SIGMA Clermont, ICCF, F-63000, Clermont-  
10                    Ferrand, France

11  
12                    (c) Laboratory of Materials Physics, Faculty of Physics, University of Science and  
13                    Technology Houari Boumediène, BP 32 El-Alia, 16111, Algiers, Algeria.

14  
15                    (d) Laboratory of Storage and Valorization of Renewable Energies, Faculty of Chemistry,  
16                    University of Science and Technology Houari Boumediène, BP 32 El-Alia, 16111,  
17                    Algiers, Algeria.

## 18 19 20                    **Abstract**

21                    In this study, the ability of Ag<sub>3</sub>PO<sub>4</sub> to achieve the photocatalytic degradation of quinoline  
22                    yellow (QY) a hazardous and recalcitrant dye, under UVA and visible light was investigated.  
23                    The photocatalyst Ag<sub>3</sub>PO<sub>4</sub> was synthesized through a precipitation method, and characterized  
24                    by X-ray diffraction (XRD), scanning electron microscope (SEM), BET Brunauer-Emmett-  
25                    Teller (BET) analysis, UV- Differential Reflectance Spectroscopy (DRS) and Fourier  
26                    transform infrared spectroscopy (FTIR). Ag<sub>3</sub>PO<sub>4</sub> could successfully induce the photocatalytic  
27                    degradation of QY under UVA and visible light. Optimal parameters were 0.5 g.L<sup>-1</sup> of the  
28                    catalyst, 20 ppm of QY and pH~7. Ag<sub>3</sub>PO<sub>4</sub> was 1.6-times more efficient than TiO<sub>2</sub> Degussa  
29                    P25 under UV<sub>A</sub> light in degrading QY. Total organic carbon (TOC) analyses confirmed the  
30                    almost complete QY mineralization. At least 8 intermediate degradation products were

31 identified by liquid chromatography coupled to high resolution mass spectrometry. The  
32 stability of  $\text{Ag}_3\text{PO}_4$  was satisfactory as less than 5% Ag metal appeared in XRD analyses after  
33 3 reuse cycles. These results show that under optimized conditions  $\text{Ag}_3\text{PO}_4$  can efficiently  
34 achieve quinolone yellow mineralization.

35 **Keywords:**  $\text{Ag}_3\text{PO}_4$ , visible light, dye, Photocatalysis, Photoproducts

36

### 37 **1. Introduction**

38 Advanced Oxidation Processes (AOPs), especially heterogeneous photocatalysis, is an  
39 environmentally friendly technique [1] that is used for pollutants elimination in water and air  
40 [2], bacterial inactivation [3], reduction of heavy metals to less harmful species and water  
41 splitting [4]. Photocatalysis initiates oxidation reactions through the generation of holes ( $\text{h}^+$ )  
42 and electrons ( $\text{e}^-$ ) pairs. The resulting radicals act as oxidants of organic pollutants and  
43 convert them into  $\text{CO}_2$ ,  $\text{H}_2\text{O}$  and inorganic salts [5]. For this reason, extensive investigation  
44 was directed toward semiconducting materials which have positive points like the  
45 environmental safety and facile preparation. On the other hand, popular photocatalysts such as  
46  $\text{ZnO}$  [6],  $\text{TiO}_2$  [7,8], and  $\text{SnO}_2$  are attractive because of their low cost, environmental  
47 friendliness [4], thermal stability and bio safe property [9,10]. However, because they possess  
48 a wide gap ( $E_g > 3 \text{ eV}$ ), their efficacy and sensitivity only occur under UV-light making  
49 solar-light application not enough efficient [11, 12]. In this respect, active research is directed  
50 to the elaboration of catalysts active under visible light for the wastewaters treatment [13-15].

51 Recently,  $\text{Ag}_3\text{PO}_4$  has gained great attention as a photocatalyst [16]. It exhibits a high  
52 photocatalytic activity upon visible-light irradiation for organic pollutants decomposition [17-  
53 20] and selective oxidation of alcohols [18]. Its photocatalytic properties depend on  
54 morphology, and active surface area [21-23]. The photocatalytic degradation of anionic dyes  
55 by  $\text{Ag}_3\text{PO}_4$  was reported to involve the photogenerated holes that show a high oxidation

56 capability in the valence band [24]. In addition, the existence of  $\text{PO}_4^{3-}$  makes easy the  
57 separation of electrons and holes ( $e^-/h^+$ ) pairs through the interfacial junction electric field  
58 which generates a dipolar moment.  $\text{Ag}_3\text{PO}_4$  synthesized by a one step process has shown that  
59 both the free radicals and the photo holes generated contribute to the dyes mineralization [22].  
60 For application of photocatalysis process in the environmental protection, it is important to  
61 use cheap, easily synthesized or readily available photocatalyst.

62 Dyes are widely used in food and cosmetic products as well as in the textile industries  
63 for their variety of colors and their chemical stability. The production of synthetic dyes  
64 exceeds 700 000 tons per year among which 140000 tons are released in the effluents in a  
65 non-controlled way [25]. Given their toxicity [26], these dyes represent an important source of  
66 pollution and a serious threat for the aquatic environment [27]. Many dyes show a high  
67 stability against temperature, light and biodegradation [28] making their elimination a major  
68 challenge in the water treatment processes. Physico-chemical treatments  
69 (coagulation/filtration, coagulation/flocculation, adsorption, etc.) are currently used for the  
70 elimination of industrial effluents [26]. However, such techniques do not degrade  
71 contaminants but only transfer them from a liquid phase to the solid phase, and additional  
72 treatments are thus required [30].

73 Quinoline Yellow (QY) is a synthetic dye and one of the most employed food  
74 additives, even though it has also applications in cosmetic and pharmaceuticals preparations  
75 [31]. This dye may cause some diseases like dermatitis and allergic reactions, and has been  
76 banned by the standards of the food industry in countries like USA, Australia, Norway and  
77 Iran [32,33]. Many N-containing dyes like QY undergo natural anaerobic reductive  
78 degradation, which can generate aromatic amines suspected to be carcinogenic [26]. For these  
79 reasons, it is necessary to undertake investigations aiming to eliminate it from water  
80 resources. Several studies concerning QY heterogeneous photocatalysis were investigated

81 using ZnO [34], TiO<sub>2</sub> [34,35] and TiO<sub>2</sub>/polyaniline composite [36]. However, to our  
82 knowledge, product studies are scarce.

83 Here, we investigated the photocatalytic degradation of QY using Ag<sub>3</sub>PO<sub>4</sub> as a  
84 photocatalyst. Ag<sub>3</sub>PO<sub>4</sub> was elaborated by a facile method at room temperature, namely the  
85 precipitation. The first part of this paper concerns the physical characterization of the material  
86 using XRD, SEM, DRS, BET method, and FTIR spectroscopy. It is complementary to the  
87 electrochemical properties previously reported [20]. The second part of this paper is focused  
88 on the optimization of operating parameters such as pH, catalyst dose and QY initial  
89 concentration. Then, photoproducts were characterized by means of ultrafast high-pressure  
90 liquid chromatography (UHPLC) coupled to electrospray ionization high-resolution mass  
91 spectrometry (ESI-HRMS), while mineralization and the photocatalyst stability were also  
92 carried out.

93

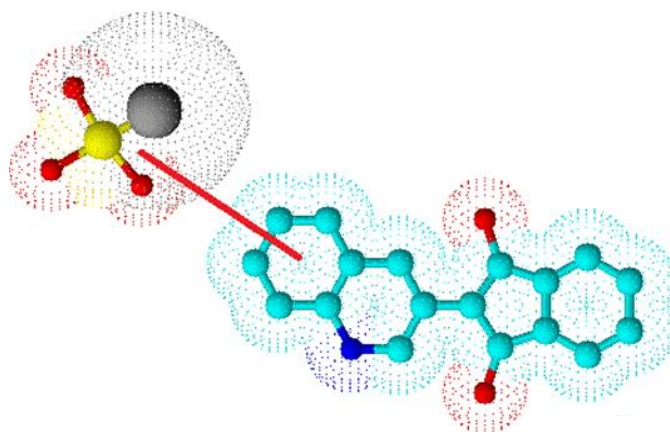
## 94 **2. Experimental**

### 95 **2.1. Chemicals**

96 Quinoline Yellow was a mixture of the mono- and disulfonic acids (acid yellow 3, Sigma-  
97 Aldrich, Fig. 1). The other chemicals were: titanium dioxide Degussa P25 (TiO<sub>2</sub> P25,99.5%,  
98 Evonik), disodium phosphate (Na<sub>2</sub>HPO<sub>4</sub>,99%, Merck), silver nitrate (AgNO<sub>3</sub>, 99.9%, Alfa  
99 Aeser), sodium hydroxide (NaOH, 99.99%, Sigma-Aldrich), perchloric acid (HClO<sub>4</sub>, 99.99%,  
100 Sigma-Aldrich), sodium acetate for HPLC LiChropur (C<sub>2</sub>H<sub>3</sub>NaO<sub>2</sub>, ≥99%, Supelco), potassium  
101 bromide FT-IR grade (KBr, 99%, Merck), formic acid for LC-MS LiChropur (CO<sub>2</sub>H<sub>2</sub>, 98% -  
102 100%, Supelco), acetonitrile LiChrosolv hyper grade for LC-MS (CH<sub>3</sub>CN, Merck) and  
103 acetonitrile gradient grade for HPLC ACS (≥ 99.9 %, Carlo Erba). All reagents were used  
104 without any purification process. Water was purified using a RIOS 5 reverse osmosis and  
105 synergy (Millipore) device (resistivity 18 MΩ.cm, DOC < 0.1 mg.L<sup>-1</sup>).

## 106 2.2. Synthesis of Ag<sub>3</sub>PO<sub>4</sub>

107 Ag<sub>3</sub>PO<sub>4</sub> was prepared by precipitation as previously described [20]. Briefly, 15 mL of a  
108 Na<sub>2</sub>HPO<sub>4</sub> solution (3 mM) was mixed dropwise to 30 mL of AgNO<sub>3</sub> solution (3 mM) under  
109 magnetic stirring during 3 h at room temperature. The precipitate with a yellow color  
110 characteristic of Ag<sub>3</sub>PO<sub>4</sub>, was collected and washed with deionized water and ethanol. The  
111 yellow powder was recovered after drying at 70 °C under static vacuum overnight.



112

113 **Fig. 1** Quinoline Yellow structure using ChemSketch software

## 114 2.3. Characterization of Ag<sub>3</sub>PO<sub>4</sub>

115 The synthesized phase was confirmed by X-ray diffraction using Co K $\alpha$  line ( $\lambda= 1.790300 \text{ \AA}$ )  
116 at a  $2\theta$  scan rate of 2 per min. The micrograph of the sample was examined by SEM analysis  
117 using a JEOL microscope (Model JSM 6360- LV). The BET surface area and pore volume  
118 were calculated from the N<sub>2</sub> adsorption/desorption isotherm at 77K using an ASAP 2010  
119 Micrometrics equipment. The external surface area, micropore area and micropore volume  
120 were computed by the t-plot technique. The total pore volume was determined from the liquid  
121 N<sub>2</sub> volume at high relative pressure (0.99). The subtraction of the micropore volume from the  
122 total volume gave the volume of mesopore. The DRS was measured using a  
123 spectrophotometer (Specord 200 Plus). The concentration of Ag before and after recycling in  
124 hydrolyzed samples was determined using Atomic Absorption Spectrophotometry (AAS)

125 (Perkin-Elmer A700). A calibration curve was created by analyzing Ag (1, 2, 3, 4  $\mu\text{g}\cdot\text{mL}^{-1}$ )  
126 standard solutions, and the instrument was adjusted to 328.1 nm.

#### 127 **2.4. Photocatalytic experiments**

128 Irradiations were conducted in two devices; one was equipped with fluorescent tubes (Philips  
129 HPK 15 W) emitting in the near UV region (maximum at 365 nm) while the other with LED  
130 (Delleled 5W) emitting within the wavelength range 400-800 nm. Pyrex reactors were  
131 connected to a thermostatically controlled water bath. For irradiation under visible 50 mL of  
132 suspensions containing  $\text{Ag}_3\text{PO}_4$  and QY were added to the reactor of 100 mL of capacity  
133 while for UVA irradiation 15 mL of suspensions were placed in the reactor of 30 mL  
134 capacity. Solution pH was adjusted using NaOH or  $\text{HClO}_4$ . In both systems, the suspensions  
135 were kept at 25 °C under constant agitation (600 rpm). Aliquots of 0.5 mL were regularly  
136 withdrawn, vigorously centrifuged and filtered through a 0.45  $\mu\text{m}$  filter (Waters, Millipore)  
137 before analyses. The degradation yield (%) was evaluated from the relationship:

$$138 \text{ Degradation in } \% = \frac{C_0 - C_t}{C_0} \times 100$$

139 (1)

140  $C_0$  being the initial QY concentration and  $C_t$  the concentration at time (t).

#### 141 **2.5 Analytical Analyses**

142 A UV-vis spectrophotometer (Model Specord 200 plus) was used to monitor the degradation  
143 of QY ( $\lambda_{\text{max}} = 434 \text{ nm}$ ). QY and its photoproducts were separated using a Shimadzu 8040  
144 HPLC system, equipped with a SPD-M30A DAD detector, and a Nucleodur 100-3  $\text{C}_{18}$  end-  
145 capped column (125 mm $\times$ 4.0 mm, 3  $\mu\text{m}$  particle size). The mobile phase was a mixture of (A)  
146 30 mmol.L<sup>-1</sup> sodium acetate and (B) acetonitrile in the proportions of 80% A and 20% B, at a  
147 constant flow rate of 0.75 mL.min<sup>-1</sup>. The detection wavelength was set at 290 nm and the  
148 temperature oven at 30 °C.

149 UHPLC-ESI-HRMS was performed on an Orbitrap Q-Exactive (Thermo Scientific) mass  
150 spectrometer coupled to a Ultimate 3000 RSLC (Thermo Scientific) apparatus. The mass  
151 spectrometer with heated electrospray ionization was operated in both positive and negative  
152 ESI modes with a spray voltage of 3 kV for both modes. The column was a Waters analytical  
153 column (2.1 mm×100 mm, 1.7 μm particle size) and the column oven temperature was  
154 regulated at 30 °C. The aqueous solvent (A) was a mixture of formic acid (0.1%) and  
155 acetonitrile as organic phase (B). The separation was achieved using a gradient program  
156 consisting of 0-7.5 min 5%, 7.5-8.5 min 99% of the mobile phase B. The injection volume  
157 was taken at 10 μL while the flow rate was fixed at 0.450 mL.min<sup>-1</sup>.

158 A Shimadzu 5050 TOC analyzer was used to monitor the mineralization of QY. The  
159 percentage of mineralization was calculated using the following equation:

$$160 \text{ Mineralization} = \frac{(OC_0 - OC_t)}{OC_0} \times 100$$

161 (2)

162 where OC<sub>0</sub> is the organic carbon present in the solution at time 0 and OC<sub>t</sub> at time t. OC is  
163 obtained by subtracting the inorganic carbon from total carbon.

164

### 165 **3. Results and discussion**

#### 166 **3.1. Characterization of Ag<sub>3</sub>PO<sub>4</sub>**

167 The XRD pattern of Ag<sub>3</sub>PO<sub>4</sub> had narrow peaks, characteristic of a high crystallization (Fig. 2  
168 a). The simulated and the measured diffractograms showed a good fit of 1.6 with R<sub>wp</sub> and R<sub>exp</sub>  
169 (%) less than 10% (Fig. 2b). The microstructural parameters obtained after the Rietveld  
170 refinement were used to determine the dislocation density after elaboration. The coherent  
171 domains of diffraction (D<sub>v</sub>) had an average value of 178 nm and the corresponding  
172 microstrain (ε) a percentage of 2.5×10<sup>-3</sup>. It is well known that the presence of crystallographic  
173 defects, such as dislocations, has a strong influence on the properties of materials. The

174 dislocation density ( $\rho$ ) calculated from equations (3, 4, 5) was  $\rho= 2.6\times 10^{12}$  in this work. This  
 175 value is acceptable and confirm the crystal quality. During the elaboration, the dislocation  
 176 assisted slip activities occurred in the studied material. In addition, the processes used in this  
 177 study had no effect on the lattice parameters ( $a= 6.0316$  nm in this work), variation of which  
 178 is only sensitive to the effects of electronic linkages of the chemical species.

$$179 \rho=(\rho_D\rho_\varepsilon)^{1/2}$$

180 (3)

181 Where  $\rho_D$  and  $\rho_\varepsilon$  are calculated using eq 4 and 5:

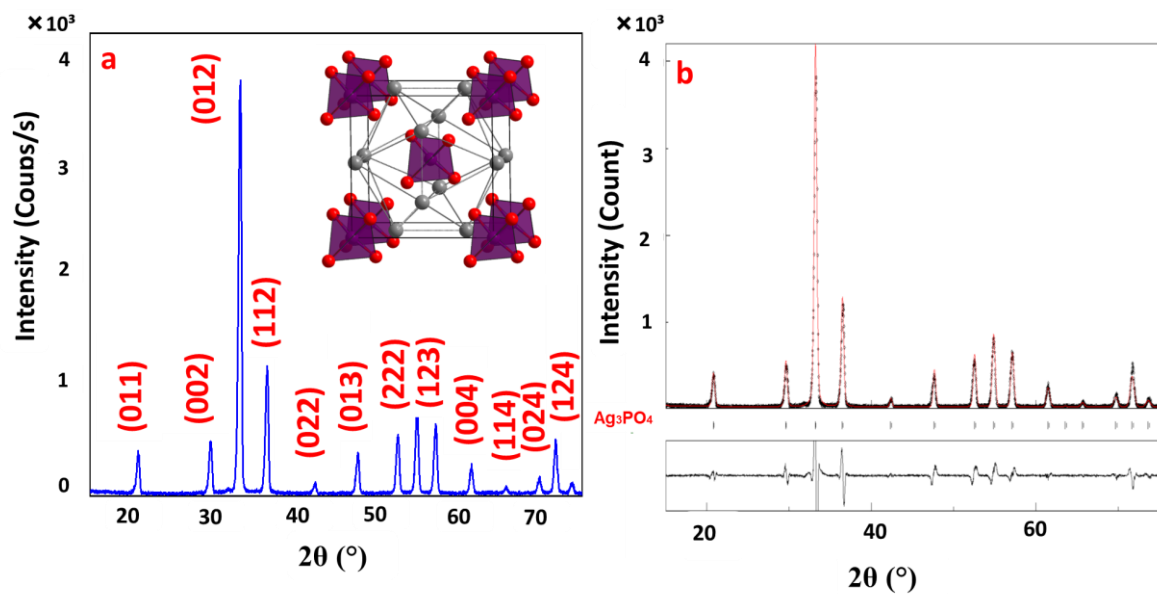
$$182 \rho_D= \frac{3}{Dv^2}$$

183 (4)

$$184 \rho_\varepsilon= \frac{2K\varepsilon^2}{b^2}$$

185 (5)

186  $b$  the Burger vector, and  $K$  is a constant equal to 10 for a Gaussian distribution of the  
 187 deformations.

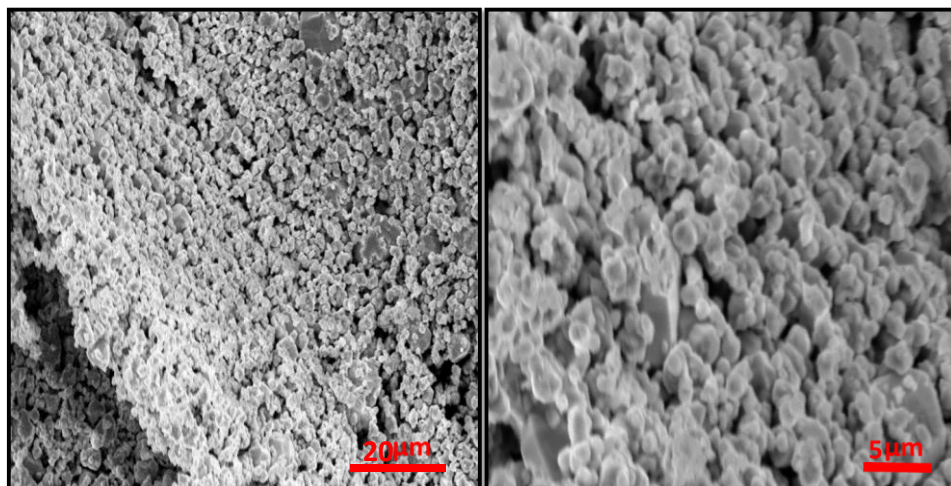


188

189 **Fig. 2.** XRD spectrum: Identified atomic plane of the  $Ag_3PO_4$  phase (a).

190 Rietveld refinement of the  $Ag_3PO_4$  phase (b)

191



192

193

**Fig. 3.** SEM images of  $\text{Ag}_3\text{PO}_4$

194

The SEM micrographs of  $\text{Ag}_3\text{PO}_4$  are illustrated in Fig. 3. It can be observed that the

Sample	Surface area ( $\text{m}^2 \cdot \text{g}^{-1}$ )			Pore volume ( $\text{cm}^3 \cdot \text{g}^{-1}$ )		
	$S_{\text{BET}}$	$S_{\text{ext}}$	$S_{\text{mic}}$	$V_{\text{T}}$	$V_{\text{mes}}$	$M_{\text{mic}}$
$\text{Ag}_3\text{PO}_4$	6	5.18	0.82	0.0192	0.0188	0.0004

195 morphology of the powder was uniform and agglomerated in spherical grains with regular

196 size lying between 1 and 1.5  $\mu\text{m}$ . The particles surface was relatively smooth. The  $\text{N}_2$ 197 adsorption-desorption isotherm of  $\text{Ag}_3\text{PO}_4$  is shown in Fig. 4. The isotherm belonged to the

198 type IV according to IUPAC classification, which indicates a well-developed mesoporous

199 nature. In addition, the desorption isotherm showed a H3-hysteresis, characteristic of a

200 capillary condensation observed in mesoporous structures [36]. The detailed textural

201 parameters of  $\text{Ag}_3\text{PO}_4$  are gathered in Table 1. The specific surface area and total pore202 volume were equal to  $6 \text{ m}^2 \cdot \text{g}^{-1}$  and  $0.0192 \text{ cm}^3 \cdot \text{g}^{-1}$ , respectively.

203

**Table 1.** Textural characteristics of  $\text{Ag}_3\text{PO}_4$

204

205

206

207

208 The formation of  $\text{Ag}_3\text{PO}_4$  was further supported by the FTIR spectroscopy, using the  
209 routine KBr technique in the  $400 - 4500 \text{ cm}^{-1}$  region. The peaks centered at  $545$  and  $1082 \text{ cm}^{-1}$   
210 <sup>1</sup> (Fig. 5) were assigned to molecular vibrations of P-O of the phosphate ( $\text{PO}_4^{3-}$ ) unit [18], and  
211 the bands at  $3401$  and  $1641 \text{ cm}^{-1}$  were attributed to the stretching vibration of O-H groups of  
212 adsorbed water. The  $\text{H}_2\text{O}$  molecules and OH groups adsorbed on the surface of  $\text{Ag}_3\text{PO}_4$  are  
213 oxidized into free hydroxyl radicals that achieve the photodegradation of organic pollutants  
214 [37]. The intense peak at  $1383 \text{ cm}^{-1}$  corresponded to the nitrate impurity,  $\text{AgNO}_3$  having been  
215 used for the preparation of  $\text{Ag}_3\text{PO}_4$  [38].

216 The knowledge of the gap band ( $E_g$ ) is of great utility in the solar energy conversion; it is  
217 evaluated from DRS by using the known relationship:

$$218 (\alpha_\lambda h\nu)^k = \text{Constant} \times (h\nu - E_g) \quad (6)$$

219  $\alpha_\lambda (\text{cm}^{-1})$  is the optical adsorption coefficient and  $h\nu$  (eV) the energy of the incident photon.  
220 The nature of the optical allowed transition is deduced from the exponent  $k$  ( $= 2$ , direct) or  
221 ( $0.5$ , indirect). The gap  $E_g$  is deduced from the intersection of the plot  $(\alpha h\nu)^2$  with the  
222 abscissa-axis. The direct transition at  $2.52 \text{ eV}$  (Fig. 6) was in conformity with the yellow color  
223 of  $\text{Ag}_3\text{PO}_4$  that is a promising photocatalyst under visible light [20].

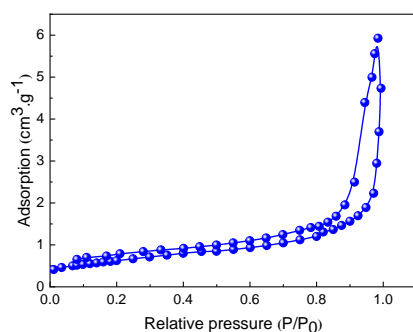


**Fig. 4.** BET of  $\text{Ag}_3\text{PO}_4$  at 77 K

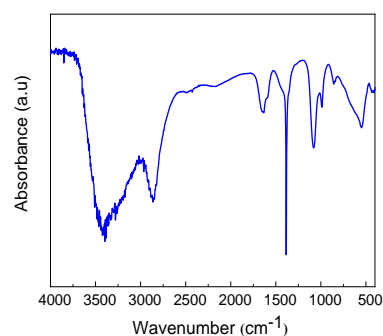


**Fig. 5.** FTIR spectrum of  $\text{Ag}_3\text{PO}_4$

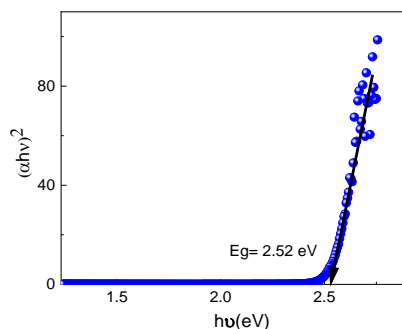


**Fig. 6.** Direct optical transition of  $\text{Ag}_3\text{PO}_4$

224

### 225 **3.2. Photocatalytic degradation of QY**

226 Neither the irradiation of QY under UVA for 4 h in absence of  $\text{Ag}_3\text{PO}_4$  nor the stirring  
 227 of QY solution pH 7 in presence of  $\text{Ag}_3\text{PO}_4$  in the dark for 24 h led to a significant  
 228 concentration loss. These results demonstrated that direct photolysis and adsorption on the  
 229 photocatalyst were negligible in these conditions. The very poor adsorption of QY on  $\text{Ag}_3\text{PO}_4$   
 230 in neutral medium can be explained by electrostatic repulsion between the negatively charged  
 231 surface of the photocatalyst and anionic QY as observed for methyl orange and orange G [39].  
 232 In contrast, when the suspension containing  $\text{Ag}_3\text{PO}_4$  and QY was exposed to UVA or visible  
 233 light, an almost complete degradation was achieved within 40 min and 70 min under visible  
 234 light and UVA, respectively (Fig. 7). Experiments were then undertaken to optimize  
 235 parameters.

#### 236 **3.2.1. Parameters optimization**

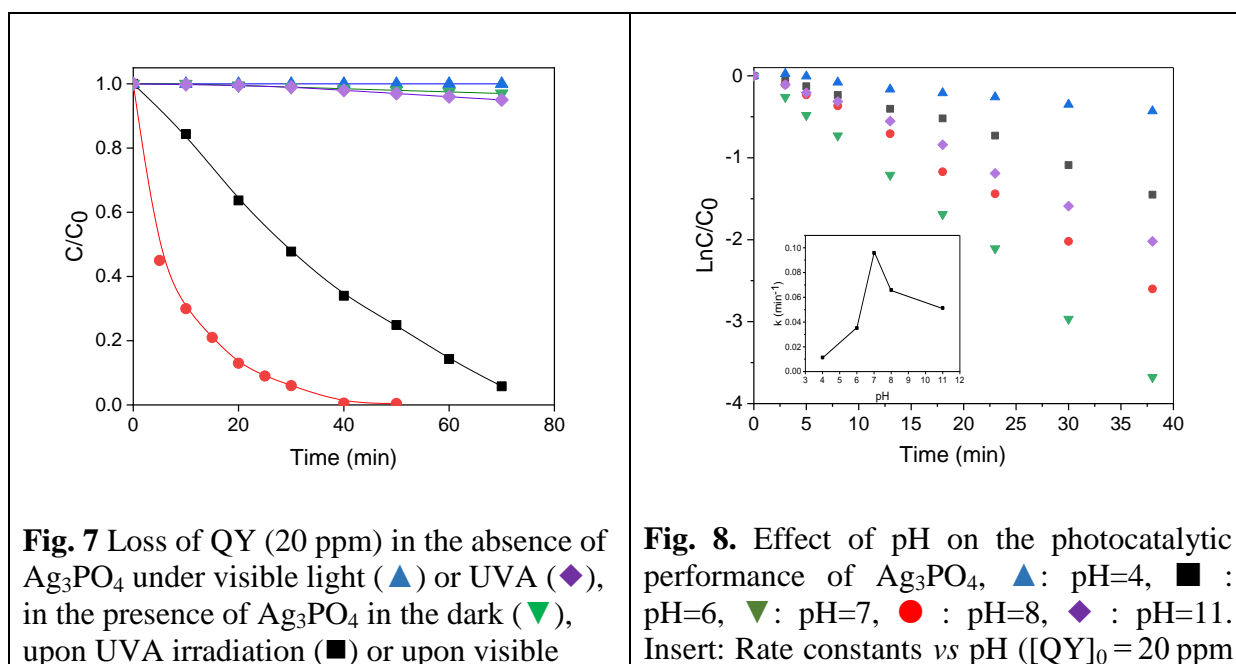
237 In this set of experiments,  $\text{Ag}_3\text{PO}_4$  suspensions were irradiated with visible light. The  
 238 degradation profile of QY was monitored until 40 min. The QY decrease rate,  $r$ , obeyed an  
 239 apparent pseudo-first order model ( $r = k \times C$ ), therefore the degradation rate constants,  $k$ ,  
 240 were obtained from the slope of the plots  $\ln(C/C_0)$  vs irradiation time.

241 The photocatalytic degradation of QY (20 ppm) by  $\text{Ag}_3\text{PO}_4$  ( $0.5 \text{ g.L}^{-1}$ ) was studied by  
 242 varying pH in the range of 4-11. As shown in Fig. 8, the degradation rate of QY was pH-

243 dependent. The highest rate constant ( $0.094 \text{ min}^{-1}$ ) was observed at pH 7. The rate constant  
 244 drastically decreased below pH 7 by 65-90% while by 40-50% above (Fig. 8). This highest  
 245 efficiency at neutral pH, close to the natural environment, is a very positive point in terms of  
 246 application.

247 The reaction was also studied at QY concentrations in the range of 5 - 40 ppm, at a  
 248 fixed dose of  $\text{Ag}_3\text{PO}_4$  ( $0.5 \text{ g.L}^{-1}$ ) and at pH 7. Between 5 and 20 ppm, the rate constant laid  
 249 between  $0.065$  and  $0.072 \text{ min}^{-1}$ , while at 30 and 40 ppm the value dropped to  $0.02$  and  $0.011$   
 250  $\text{min}^{-1}$ , respectively. At 40 ppm, the absorbance of the QY solution was equal to 3.2 at 434 nm,  
 251 QY had therefore a very strong filter effect and prevents  $\text{Ag}_3\text{PO}_4$  to absorb light.

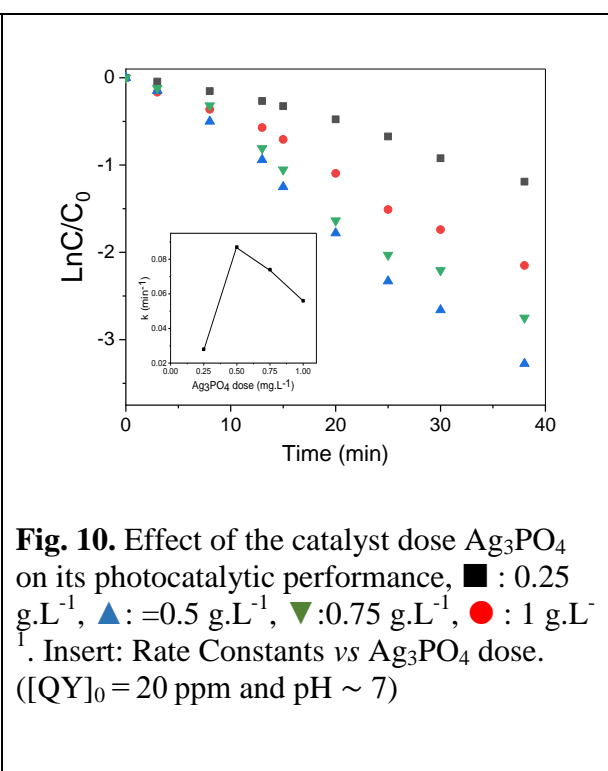
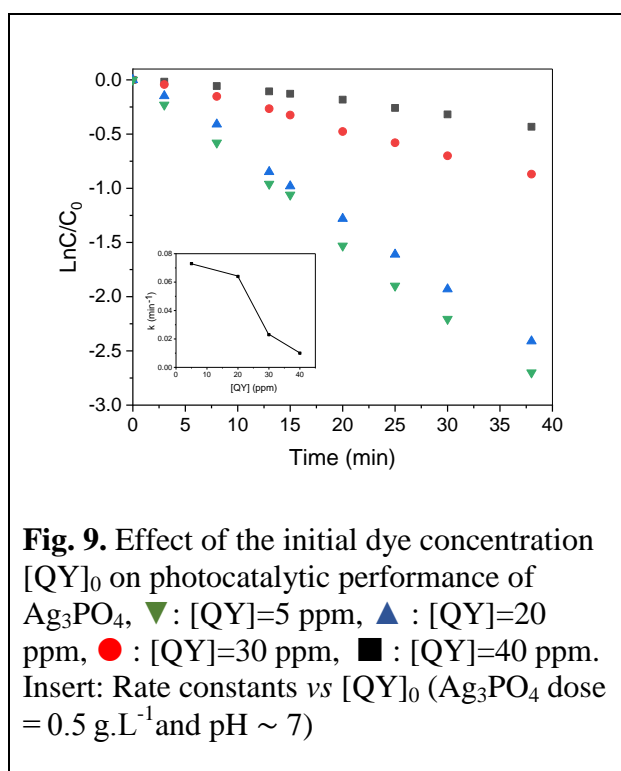
252 The  $\text{Ag}_3\text{PO}_4$  photocatalyst dose was varied in the range of  $0.25 - 1 \text{ g.L}^{-1}$  to avoid the  
 253 photocatalyst excess and ensure a total absorption of efficient incident photons. Fig. 10 shows  
 254 that the degradation rate increased with the catalyst dose and reached a maximum for  $0.5 \text{ g.L}^{-1}$ .  
 255 The rate constant  $k$  was equal to  $8.6 \text{ min}^{-1}$ . An increase of the catalyst dose up to  $1.5 \text{ g.L}^{-1}$   
 256 led to a reduced photoactivity due to a lower availability of photoactive sites on the  $\text{Ag}_3\text{PO}_4$   
 257 surface and a weak light utilization [40]. The optimal conditions ( $\text{Ag}_3\text{PO}_4$  dose =  $0.5 \text{ g.L}^{-1}$ ,  
 258  $[\text{QY}] = 20 \text{ ppm}$  and  $\text{pH} \sim 7$ ) were kept for experiments under UVA irradiation.



light (●).([QY]<sub>0</sub> = 20 ppm, Ag<sub>3</sub>PO<sub>4</sub>  
dose = 0.5 g.L<sup>-1</sup> and pH ~ 7)

and Ag<sub>3</sub>PO<sub>4</sub> dose = 0.5 g.L<sup>-1</sup>)

Conditions	k( min <sup>-1</sup> )	R <sup>2</sup>	Reference
------------	------------------------	----------------	-----------



259

### 260 3.2.2. Compared photocatalytic activity Ag<sub>3</sub>PO<sub>4</sub> /TiO<sub>2</sub> Degussa P25

261 The photocatalytic efficiency Ag<sub>3</sub>PO<sub>4</sub> and TiO<sub>2</sub> Degussa P25 were compared at the  
262 dose of 0.5 g.L<sup>-1</sup>. Under visible light Ag<sub>3</sub>PO<sub>4</sub> was active while TiO<sub>2</sub> non active and under  
263 UVA, Ag<sub>3</sub>PO<sub>4</sub> was 1.6-times more efficient than TiO<sub>2</sub>. This demonstrates the interest of  
264 Ag<sub>3</sub>PO<sub>4</sub> as a photocatalyst.

265 **Table 2.** QY degradation rate constants (*k*) using Ag<sub>3</sub>PO<sub>4</sub> (0.5 g.L<sup>-1</sup>) or TiO<sub>2</sub> Degussa P25  
266 (0.5 g.L<sup>-1</sup>) as a photocatalyst

267	TiO <sub>2</sub> Degussa P25 + QY + UVA	0.018	0.998	This work
	Ag <sub>3</sub> PO <sub>4</sub> + QY + UVA	0.029	0.987	This work
268	Ag <sub>3</sub> PO <sub>4</sub> + QY + Visible light	0.099	0.992	This work
269	TiO <sub>2</sub> Degussa P25 + QY + Visible light	<1.8 × 10 <sup>-4</sup>		This work

270

271

### 272 3.3 Product studies

273 HPLC and UHPLC-ESI-HRMS analyses were conducted for products identification.

274 QY is sold by Sigma-Aldrich as a mixture of mono and disulfonic acids C<sub>18</sub>H<sub>12</sub>NO<sub>5</sub>SNa -

275 C<sub>18</sub>H<sub>11</sub>NO<sub>8</sub>S<sub>2</sub>Na<sub>2</sub>. Yet, we only detected two peaks at m/z = 353.0352 in ES<sup>-</sup>. They

276 correspond to two isomeric forms of the monosulfonic acid (Fig. 11 a, Fig. 11 b). Three

277 samples were analyzed after 44, 70 and 175 min of irradiation under UVA. In the first two

278 samples the QY conversion extent was of 50% and 80% and in the third one QY was fully

279 degraded (Fig.11 c). A typical HPLC chromatogram is shown Fig. 11c and Table 3 gives the

280 accurate and experimental m/z, the chemical formula in the limit of 5 ppm and the possible

281 structure of the 8 detected photoproducts (TPs) by UHPLC-ESI-HRMS. In general, TPs were

282 detected by negative electro spray ionization.

283 TP1 showed m/z = 208.0074 corresponding to C<sub>9</sub>H<sub>7</sub>O<sub>3</sub>NS for the neutral molecule. This TP

284 was likely quinoline sulfonic acid formed by C-C cleavage and its detection allowed us to

285 locate the sulfonic group of QY on the quinoline ring. With m/z = 251.9977, TP2 had the

286 molecular formula of C<sub>10</sub>H<sub>7</sub>O<sub>5</sub>N and corresponded to TP1+CO<sub>2</sub>. It was therefore likely a

287 carboxylated

288

289

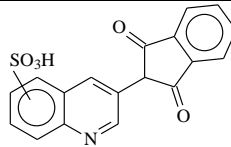
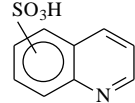
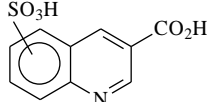
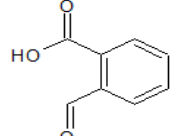
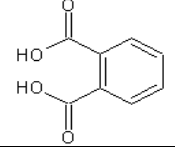
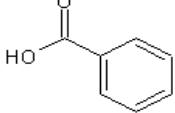
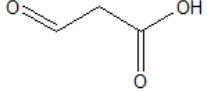
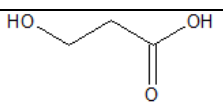
290

291

292

**Table 3.** UHPLC-HRMS data of QY-Ag<sub>3</sub>PO<sub>4</sub> irradiated under UVA

Compound	Accurate m/z of [M-H] <sup>-</sup>	Exp. m/z of [M-H] <sup>-</sup>	Δppm	Chemical formula	Proposed chemical structure
----------	------------------------------------	--------------------------------	------	------------------	-----------------------------

Quinoline Yellow	353.0352	353.0287	1.84	C <sub>18</sub> H <sub>11</sub> O <sub>5</sub> NS	
TP1	208.0063	208.0074	-2.95	C <sub>9</sub> H <sub>7</sub> O <sub>3</sub> NS	
TP2	251.9961	251.9977	-4.96	C <sub>10</sub> H <sub>7</sub> O <sub>5</sub> NS	
TP3	149.0233	149.0229	2.68	C <sub>8</sub> H <sub>6</sub> O <sub>3</sub>	
TP4	165.0182	165.0187	-3.03	C <sub>8</sub> H <sub>6</sub> O <sub>4</sub>	
TP5	121.0284	121.0286	-1.65	C <sub>7</sub> H <sub>6</sub> O <sub>2</sub>	
TP6	89.0233	89.0231	2.24	C <sub>3</sub> H <sub>6</sub> O <sub>3</sub>	
TP7	87.0077	87.0074	3.45	C <sub>3</sub> H <sub>4</sub> O <sub>3</sub>	
TP8	61.9873	61.9868	-4.6	NO <sub>3</sub> <sup>-</sup>	

293

294

295 quinoline sulfonic acid formed by cleavage of the 5-carbon ring. TP3 with m/z = 149.0229

296 corresponded to a molecular formula of C<sub>8</sub>H<sub>6</sub>O<sub>3</sub>. On the other hand, TP4 that showed m/z =

297 165.018 corresponded to C<sub>8</sub>H<sub>6</sub>O<sub>4</sub> and most probably to phthalic acid. TP3 might be therefore

298 the corresponding aldehyde. TP5 was identified to benzoic acid (m/z = 121.0286 and

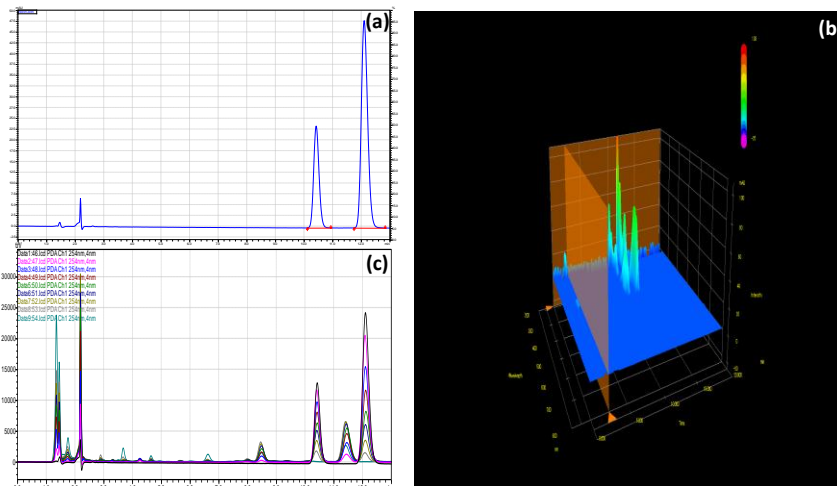
299 C<sub>7</sub>H<sub>6</sub>O<sub>2</sub>). TP6 and TP7 with m/z = 89.0231 and 87.0074 were two aliphatic acids with 3

300 atoms of carbon produced by oxidation and opening of the rings. Nitrate ions (m/z = 62.0049)

301 were also detected. TP1-TP5 were detected after 44 and 70 min of irradiation while TP6, TP7

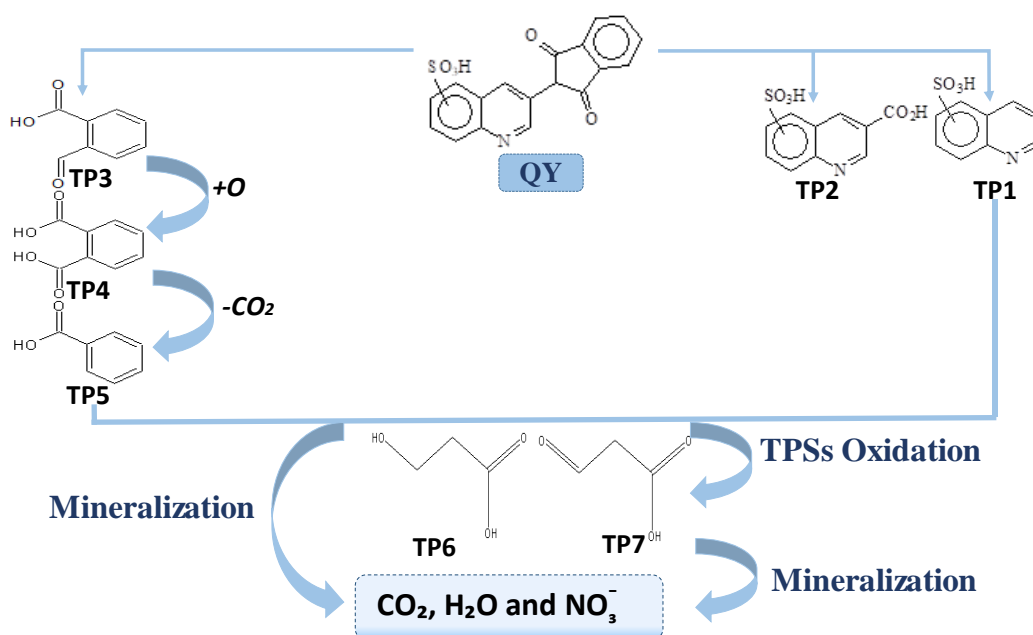
302 and nitrate ions in the samples irradiated for 175 min. The degradation pathways are  
 303 summarized in Fig.12.

304



305

306 **Fig. 11** 2D HPLC chromatogram (a) and 3D HPLC chromatogram (b) of QY of mono-  
 307 sulfonic acid of QY isomers. HPLC chromatogram of photodegraded QY solution (c)  
 308 ([QY]<sub>0</sub> = 20 ppm, Ag<sub>3</sub>PO<sub>4</sub> dose = 0.5 g.L<sup>-1</sup> and pH ~ 7)  
 309



310

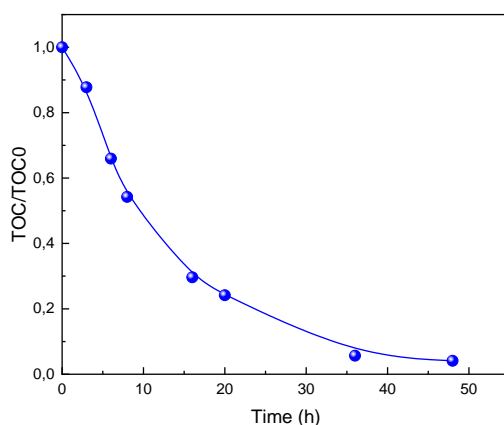
311 **Fig. 12** Proposed degradation mechanism for QY in Ag<sub>3</sub>PO<sub>4</sub> process

312

### 313 3.4. Mineralization

314 TOC evolution during the photocatalytic reaction was monitored to explore the  
 315 percentage of QY mineralization under the optimal conditions (QY 20 ppm, Ag<sub>3</sub>PO<sub>4</sub> dose

316 =0.5 g.L<sup>-1</sup> and pH 7) (Fig. 13). After 70 min of irradiation under UVA corresponding to the  
317 full degradation of QY, only 5% of OC were transformed into CO<sub>2</sub>. Total OC removal was  
318 reached after 48 h of irradiation time. This long time to achieve complete mineralization  
319 indicates that intermediates were difficult to oxidize.



320

321 **Fig. 13** Organic carbon evolution during QY photocatalytic degradation in presence of  
322 Ag<sub>3</sub>PO<sub>4</sub> under UVA. [QY]<sub>0</sub> = 20 ppm, Ag<sub>3</sub>PO<sub>4</sub> dose = 0.5 g.L<sup>-1</sup> and pH ~ 7)

### 323 3.5. Catalyst stability and reusability

324 To assess the photostability and reusability of Ag<sub>3</sub>PO<sub>4</sub> under visible irradiation for the  
325 photodegradation of QY, three photodegradation experiments were successively performed.  
326 After each cycle, the catalyst was centrifuged, filtered, thoroughly rinsed with water and  
327 ethanol and finally dried at 70°C. After three recycles, 87, 78 and 64% of QY were  
328 photodegraded (Fig. 14 a) within 40 min. These results revealed some deactivation effects.  
329 This reduction can be explained by the reduction of Ag<sup>+</sup> to metallic state Ag in the presence  
330 of photogenerated electrons. To quantify the percentage of photoreduced Ag<sup>+</sup> both XRD and  
331 AAS analyses were carried out (Table 4). XRD results after the three cycles are shown in Fig.  
332 14 b. Small peaks of Ag appeared (< 5%) [20,41]. On the other hand, results of the literature  
333 showed that when dispersed in water and irradiated under visible light for a long time,  
334 Ag<sub>3</sub>PO<sub>4</sub> remained stable (dissolution <1 ppm). Our analyses in atomic absorption  
335 spectroscopy confirmed this result (Table 4).

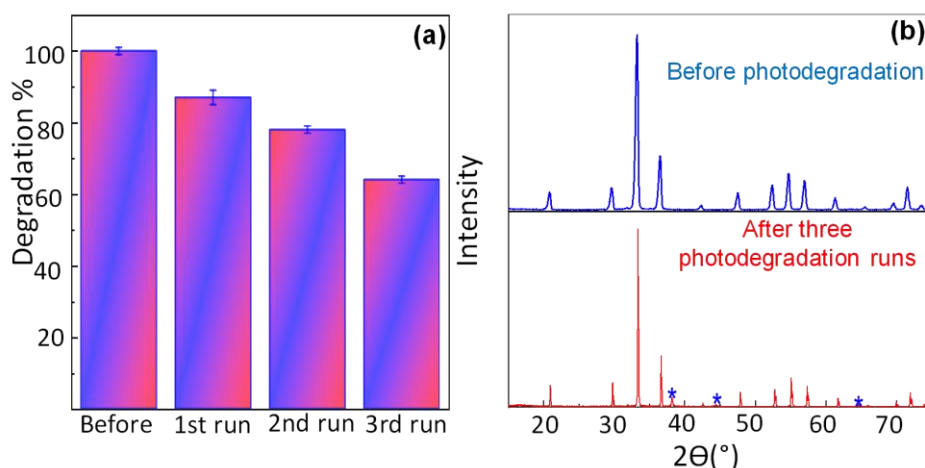


**Fig. 14** Reusability of  $\text{Ag}_3\text{PO}_4$  photocatalyst. XRD pattern after three cycles (a). Degradation yield after 40 min of irradiation under visible light for three runs (b). ( $[\text{QY}]_0 = 20$  ppm,  $\text{Ag}_3\text{PO}_4$  dose =  $0.5 \text{ g.L}^{-1}$  and  $\text{pH} \sim 7$ )

**Table 4.** Solubility of  $\text{Ag}_3\text{PO}_4$  in different conditions

$[\text{Ag}^+]^a$ (ppm) conditions	After 75 min of irradiation	After 24H of irradiation
$\text{Ag}_3\text{PO}_4$ in the dark	0.018	0.019
$\text{Ag}_3\text{PO}_4$ + Visible light	0.017	0.017
$\text{Ag}_3\text{PO}_4$ + QY + Visible light	0.02	0.02

#### 4. Conclusion

$\text{Ag}_3\text{PO}_4$  was synthesized by precipitation at ambient temperature. It was shown to induce the photocatalytic oxidation of Quinoline Yellow under visible irradiation with an efficiency much higher than that of  $\text{TiO}_2$  Degussa P25 under UVA. The optimal parameters such as initial pH, QY concentration and catalyst dose were determined. Photoproducts of QY were identified based on the UHPLC-ESI-HRMS analysis and were different than those identified using  $\text{TiO}_2$ . The complete mineralization of QY could be achieved after 48 of irradiation against 70 min for QY elimination. Some XRD peaks of Ag metal ( $\sim 5\%$ ) were noticeable after 3 reuses. It can be concluded that  $\text{Ag}_3\text{PO}_4$  needs efficient hetero-junction to avoid its photocorrosion. This is the subject of our future investigations.

357 **Acknowledgments:** A.T. thanks the Franco-Algerien “PROFAS B+” program for having  
358 granted her stay in the ICCF. The authors also thank Martin Lereboure (Engineer CNRS)  
359 and Frederic Emmenegger (Tech CNRS) for the UHPLC-HRMS analyses.

360

## 361 **References**

362

- 363 1. Yang, Y.; Li, X.; Zhou, C.; Xiong, W.; Zeng, G.; Huang, D.; Zhang, C.; Wang, W.;  
364 Song, B.; Tang, X.; Li, X.; Guo, H. Recent advances in application of graphitic carbon  
365 nitride-based catalysts for degrading organic contaminants in water through advanced  
366 oxidation processes beyond photocatalysis: A critical review. *Water Res.* **2020**, *184*,  
367 116200, doi:10.1016/j.watres.2020.116200.  
368
- 369 2. Karpuraranjith, M.; Chen, Y.; Wang, X.; Yu, B.; Rajaboopathi, S.; Yang, D.  
370 Hexagonal SnSe nanoplate supported SnO<sub>2</sub>-CNTs nanoarchitecture for enhanced  
371 photocatalytic degradation under visible light driven. *Appl. Surf. Sci.* **2020**, *507*,  
372 145026, doi:10.1016/j.apsusc.2019.145026.  
373
- 374 3. Yu, H.; Wang, D.; Zhao, B.; Lu, Y.; Wang, X.; Zhu, S.; Qin, W.; Huo, M. Enhanced  
375 photocatalytic degradation of tetracycline under visible light by using a ternary  
376 photocatalyst of Ag<sub>3</sub>PO<sub>4</sub>/AgBr/g-C<sub>3</sub>N<sub>4</sub> with dual Z-scheme heterojunction. *Sep. Purif.*  
377 *Technol.* **2020**, *237*, 116365, doi:10.1016/j.seppur.2019.116365.  
378
- 379 4. Wang, J.; Yue, X.; Yang, Y.; Sirisomboonchai, S.; Wang, P.; Ma, X.; Abudula, A.;  
380 Guan, G. Earth-abundant transition-metal-based bifunctional catalysts for overall  
381 electrochemical water splitting: A review. *J. Alloys Compd.* **2020**, *819*, 153346,  
382 doi:10.1016/j.jallcom.2019.153346.
- 383 5. Mudhoo, A.; Paliya, S.; Goswami, P.; Singh, M.; Lofrano, G.; Carotenuto, M.;  
384 Carraturo, F.; Libralato, G.; Guida, M.; Usman, M.; Kumar, S. Fabrication,  
385 functionalization and performance of doped photocatalysts for dye degradation and  
386 mineralization: a review; Springer International Publishing, 2020; Vol. 18; ISBN  
387 1031102001045.
- 388 6. Ong, C.B.; Ng, L.Y.; Mohammad, A.W. A review of ZnO nanoparticles as solar  
389 photocatalysts: Synthesis, mechanisms and applications. *Renew. Sustain. Energy Rev.*  
390 **2018**, *81*, 536–551, doi:10.1016/j.rser.2017.08.020.
- 391 7. Guo, Q.; Zhou, C.; Ma, Z.; Yang, X. Fundamentals of TiO<sub>2</sub> Photocatalysis: Concepts,  
392 Mechanisms, and Challenges. *Adv. Mater.* **2019**, *31*, 1–26,  
393 doi:10.1002/adma.201901997.
- 394 8. Vernardou, D.; Stratakis, E.; Kenanakis, G.; Yates, H.M.; Couris, S.; Pemble, M.E.;  
395 Koudoumas, E.; Katsarakis, N. One pot direct hydrothermal growth of photoactive  
396 TiO<sub>2</sub> films on glass. *J. Photochem. Photobiol. A Chem.* **2009**, *202*, 81–85,  
397 doi:10.1016/j.jphotochem.2008.11.015.
- 398 9. Chantana, J.; Kawano, Y.; Nishimura, T.; Mavlonov, A.; Minemoto, T. Impact of

- 399 Urbach energy on open-circuit voltage deficit of thin-film solar cells. *Sol. Energy*  
400 *Mater. Sol. Cells* **2020**, *210*, 110502, doi:10.1016/j.solmat.2020.110502.
- 401 10. Fatimah, I.; Nurillahi, R.; Sahroni, I.; Muraza, O. TiO<sub>2</sub>-pillared saponite and  
402 photosensitization using a ruthenium complex for photocatalytic enhancement of the  
403 photodegradation of bromophenol blue. *Appl. Clay Sci.* **2019**, *183*, 105302,  
404 doi:10.1016/j.clay.2019.105302.
- 405 11. Chen, D.; Huang, S.; Huang, R.; Zhang, Q.; Le, T.T.; Cheng, E.; Hu, Z.; Chen, Z.  
406 Convenient fabrication of Ni-doped SnO<sub>2</sub> quantum dots with improved  
407 photodegradation performance for Rhodamine B. *J. Alloys Compd.* **2019**, *788*, 929–  
408 935, doi:10.1016/j.jallcom.2019.02.193.
- 409 12. Chakraborty, S.; Farida, J.J.; Simon, R.; Kasthuri, S.; Mary, N.L. Averrho carrambola  
410 fruit extract assisted green synthesis of zno nanoparticles for the photodegradation of  
411 congo red dye. *Surfaces and Interfaces* **2020**, *19*, 100488,  
412 doi:10.1016/j.surfin.2020.100488.
- 413 13. Mallakpour, S.; Behranvand, V. *Nanocomposites based on biosafe nano ZnO and*  
414 *different polymeric matrixes for antibacterial, optical, thermal and mechanical*  
415 *applications*; Elsevier Ltd, 2016; Vol. 84; ISBN 8415683111.
- 416 14. Kadhim, I.H.; Hassan, H.A.; Ibrahim, F.T. Hydrogen gas sensing based on  
417 nanocrystalline SnO<sub>2</sub> thin films operating at low temperatures. *Int. J. Hydrogen Energy*  
418 **2020**, *45*, 25599–25607, doi:10.1016/j.ijhydene.2020.06.136.
- 419 15. Manoj Kumar, P.; Mylsamy, K.; Saravanakumar, P.T.; Anandkumar, R.; Pranav, A.  
420 Experimental Study on Thermal Properties of Nano-TiO<sub>2</sub> Embedded Paraffin (NEP)  
421 for Thermal Energy Storage Applications. *Mater. Today Proc.* **2019**, *22*, 2153–2159,  
422 doi:10.1016/j.matpr.2020.03.282.
- 423 16. Liu, L.; Hu, P.; Li, Y.; An, W.; Lu, J.; Cui, W. P3HT-coated Ag<sub>3</sub>PO<sub>4</sub> core-shell  
424 structure for enhanced photocatalysis under visible light irradiation. *Appl. Surf. Sci.*  
425 **2019**, *466*, 928–936, doi:10.1016/j.apsusc.2018.10.112.
- 426 17. Borjigin, B.; Ding, L.; Li, H.; Wang, X. A solar light-induced photo-thermal catalytic  
427 decontamination of gaseous benzene by using Ag/Ag<sub>3</sub>PO<sub>4</sub>/CeO<sub>2</sub> heterojunction. *Chem.*  
428 *Eng. J.* **2020**, *402*, 126070, doi:10.1016/j.cej.2020.126070.
- 429 18. Sedaghati, N.; Habibi-Yangjeh, A.; Pirhashemi, M.; Asadzadeh-Khaneghah, S.; Ghosh,  
430 S. Integration of BiOI and Ag<sub>3</sub>PO<sub>4</sub> nanoparticles onto oxygen vacancy rich-TiO<sub>2</sub> for  
431 efficient visible-light photocatalytic decontaminations. *J. Photochem. Photobiol. A*  
432 *Chem.* **2020**, *400*, 112659, doi:10.1016/j.jphotochem.2020.112659.
- 433 19. Boudiaf, S.; Nasrallah, N.; Mellal, M.; Belabed, C.; Belhamdi, B.; Meziani, D.; Mehdi,  
434 B.; Trari, M. Synthesis and characterization of semiconductor CoAl<sub>2</sub>O<sub>4</sub> for optical and  
435 dielectric studies: Application to photodegradation of organic pollutants under visible  
436 light. *Optik (Stuttg.)*. **2020**, *219*, 165038, doi:10.1016/j.ijleo.2020.165038.
- 437 20. Tab, A.; Bellal, B.; Belabed, C.; Dahmane, M.; Trari, M. Visible light assisted  
438 photocatalytic degradation and mineralization of Rhodamine B in aqueous solution by  
439 Ag<sub>3</sub>PO<sub>4</sub>. *Optik (Stuttg.)*. **2020**, *214*, 164858, doi:10.1016/j.ijleo.2020.164858.
- 440 21. Belabed, C.; Bellal, B.; Tab, A.; Dib, K.; Trari, M. Optical and dielectric properties for  
441 the determination of gap states of the polymer semiconductor: Application to

- 442 photodegradation of organic pollutants. *Optik (Stuttg)*. **2018**, 216, 218-226,  
443 doi:10.1016/j.ijleo.2018.01.109.
- 444 22. Liu, L.; Ding, L.; Liu, Y.; An, W.; Lin, S.; Liang, Y.; Cui, W. A stable Ag<sub>3</sub>PO<sub>4</sub>@PANI  
445 core@shell hybrid: Enrichment photocatalytic degradation with  $\pi$ - $\pi$  conjugation. *Appl.*  
446 *Catal. B Environ.* **2017**, 201, 92–104, doi:10.1016/j.apcatb.2016.08.005.
- 447 23. Belabed, C.; Rekhila, G.; Doulache, M.; Zitouni, B.; Trari, M. Photo-electrochemical  
448 characterization of polypyrrol: Application to visible light induced hydrogen  
449 production. *Sol. energy Mater. Sol. cells* **2013**, 114, 199–204,  
450 doi: 10.1016/j.solmat.2013.03.016.
- 451 24. Chiu, Y.H.; Chang, T.F.M.; Chen, C.Y.; Sone, M.; Hsu, Y.J. Mechanistic insights into  
452 photodegradation of organic dyes using heterostructure photocatalysts. *Catalysts* **2019**,  
453 9, 430, doi:10.3390/catal9050430.
- 454 25. Dias, F.F.; Oliveira, A.A.S.; Arcanjo, A.P.; Moura, F.C.C.; Pacheco, J.G.A. Residue-  
455 based iron catalyst for the degradation of textile dye via heterogeneous photo-Fenton.  
456 *Appl. Catal. B Environ.* **2016**, 186, 136–142, doi:10.1016/j.apcatb.2015.12.049.
- 457 26. Cao, Z.; Zhang, T.; Ren, P.; Cao, D.; Lin, Y.; Wang, L.; Zhang, B.; Xiang, X. Doping  
458 of chlorine from a neoprene adhesive enhances degradation efficiency of dyes by  
459 structured TiO<sub>2</sub>-coated photocatalytic fabrics. *Catalysts* **2020**, 10, 69,  
460 doi:10.3390/catal10010069.
- 461 27. Alahiane, S.; Sennaoui, A.; Sakr, F.; Dinne, M.; Qourzal, S.; Assabbane, A.  
462 Synchronous role of coupled adsorption-photocatalytic degradation of Direct Red 80  
463 with nanocrystalline TiO<sub>2</sub>-coated non-woven fibres materials in a static batch  
464 photoreactor. *Groundw. Sustain. Dev.* **2020**, 11, 100396,  
465 doi:10.1016/j.gsd.2020.100396.
- 466 28. Ebrahimi, R.; Maleki, A.; Zandsalimi, Y.; Ghanbari, R.; Shahmoradi, B.; Rezaee, R.;  
467 Safari, M.; Joo, S.W.; Daraei, H.; Harikaranahalli Puttaiah, S.; Giahi, O. Photocatalytic  
468 degradation of organic dyes using WO<sub>3</sub>-doped ZnO nanoparticles fixed on a glass  
469 surface in aqueous solution. *J. Ind. Eng. Chem.* **2019**, 73, 297–305,  
470 doi:10.1016/j.jiec.2019.01.041.
- 471 29. Kumari, M.; Gupta, S.K. A novel process of adsorption cum enhanced coagulation-  
472 flocculation spiked with magnetic nanoadsorbents for the removal of aromatic and  
473 hydrophobic fraction of natural organic matter along with turbidity from drinking  
474 water. *J. Clean. Prod.* **2020**, 244, 118899, doi:10.1016/j.jclepro.2019.118899.
- 475 30. Molavi, H.; Shojaei, A.; Pourghaderi, A. Rapid and tunable selective adsorption of  
476 dyes using thermally oxidized nanodiamond. *J. Colloid Interface Sci.* **2018**, 524, 52–  
477 64, doi:10.1016/j.jcis.2018.03.088.
- 478 31. Macioszek, V.K.; Kononowicz, A.K. The evaluation of the genotoxicity of two  
479 commonly used food colors: Quinoline Yellow (E 104) and Brilliant Black BN (E  
480 151). *Cell. Mol. Biol. Lett.* **2004**, 9, 107–122, doi:10.1016/j.cmbio.2016.01.279.
- 481 32. Lau, K.; McLean, W.G.; Williams, D.P.; Howard, C.V. Synergistic interactions  
482 between commonly used food additives in a developmental neurotoxicity test. *Toxicol.*  
483 *Sci.* **2006**, 90, 178–187, doi:10.1093/toxsci/kfj073.
- 484 33. Belabed, C.; Abdi, A.; Benabdelghani, Z.; Rekhila, G.; Etxeberria, A.; Trari, M.

- 485 Photoelectrochemical properties of doped polyaniline: Application to hydrogen  
486 photoproduction. *Int. J. Hydrogen Energy* **2013**, *38*, 6593–6599,  
487 doi:10.1016/j.ijhydene.2013.03.085.
- 488 34. Regulska, E.; Brus, D.M.; Rodziewicz, P.; Sawicka, S.; Karpinska, J. Photocatalytic  
489 degradation of hazardous Food Yellow 13 in TiO<sub>2</sub> and ZnO aqueous and river water  
490 suspensions. *Catal. Today* **2016**, *266*, 72–81, doi:10.1016/j.cattod.2015.08.010.
- 491 35. Gupta, V.K.; Jain, R.; Agarwal, S.; Nayak, A.; Shrivastava, M. Photodegradation of  
492 hazardous dye quinoline yellow catalyzed by TiO<sub>2</sub>. *J. Colloid Interface Sci.* **2012**, *366*,  
493 135–140, doi:10.1016/j.jcis.2011.08.059.
- 494 36. Salem, M.A.; Al-Ghonemiy, A.F.; Zaki, A.B. Photocatalytic degradation of Allura red  
495 and Quinoline yellow with Polyaniline/TiO<sub>2</sub> nanocomposite. *Appl. Catal. B Environ.*  
496 **2009**, *91*, 59–66, doi:10.1016/j.apcatb.2009.05.027.
- 497 37. Shen, Y.; Zhu, Z.; Wang, X.; Khan, A.; Gong, J.; Zhang, Y. Synthesis of Z-scheme g-  
498 C<sub>3</sub>N<sub>4</sub>/Ag/Ag<sub>3</sub>PO<sub>4</sub> composite for enhanced photocatalytic degradation of phenol and  
499 selective oxidation of gaseous isopropanol. *Mater. Res. Bull.* **2018**, *107*, 407–415,  
500 doi:10.1016/j.materresbull.2018.08.017.
- 501 38. Du, J.; Ma, S.; Yan, Y.; Li, K.; Zhao, F.; Zhou, J. Corn-silk-templated synthesis of  
502 TiO<sub>2</sub> nanotube arrays with Ag<sub>3</sub>PO<sub>4</sub> nanoparticles for efficient oxidation of organic  
503 pollutants and pathogenic bacteria under solar light. *Colloids Surfaces A Physicochem.*  
504 *Eng. Asp.* **2019**, *572*, 237–249, doi:10.1016/j.colsurfa.2019.04.018.
- 505 39. Luo, L.; Li, Y.; Hou, J.; Yang, Y. Visible photocatalysis and photostability of Ag<sub>3</sub>PO<sub>4</sub>  
506 photocatalyst. *Appl. Surf. Sci.* **2014**, *319*, 332–338, doi:10.1016/j.apsusc.2014.04.154.
- 507 40. Gaya, U.I.; Abdullah, A.H. Heterogeneous photocatalytic degradation of organic  
508 contaminants over titanium dioxide: A review of fundamentals, progress and problems.  
509 *J. Photochem. Photobiol. C Photochem. Rev.* **2008**, *9*, 1–12,  
510 doi:10.1016/j.jphotochemrev.2007.12.003.
- 511 41. Zhang, H.; Huang, H.; Ming, H.; Li, H.; Zhang, L.; Liu, Y.; Kang, Z. Carbon quantum  
512 dots/Ag<sub>3</sub>PO<sub>4</sub> complex photocatalysts with enhanced photocatalytic activity and stability  
513 under visible light. *J. Mater. Chem.* **2012**, *22*, 10501–10506, doi:10.1039/c2jm30703k.
- 514